Available online at www.sciencedirect.com
SCIENCE DIRECT®
Journal of Power Sources 152 (2005) 75–86
JOURNAL OF POWER SOURCES
www.elsevier.com/locate/jpowsour

Microlith catalytic reactors for reforming *iso*-octane-based fuels into hydrogen☆

Subir Roychoudhury[a,*], Marco Castaldi[a,1], Maxim Lyubovsky[a], Rene LaPierre[a], Shabbir Ahmed[b]

[a] *Precision Combustion Inc., 410 Sackett Point Road, North Haven, CT 06473, USA*
[b] *Chemical Engineering Division, Argonne National Laboratory, 9700 South Cass Avenue, Argonne, IL 60439, USA*

Received 17 December 2004; accepted 12 January 2005
Available online 12 April 2005

Abstract

Recent advances in the development of short contact time (SCT) reactor design approaches allow reformers capable of overcoming current barriers of cost, size, weight, complexity and efficiency associated with conventional reactor design approaches. PCI has developed an SCT based approach using a patented substrate (trademarked Microlith®) and proprietary coating technology [1]. The high heat and mass transport properties of the substrate have been shown to significantly reduce reactor size while improving performance. Resistance to coking, especially at low H_2O:C ratios, has also been observed with these reactors.

This paper summarizes the results of auto thermal reforming (ATR) of an *iso*-octane-based liquid fuel. In addition Microlith-based water gas shift (WGS) and preferential CO oxidation (PROX) reactors were also examined for fuel processing applications. Surprisingly, selectivity advantages for these kinetically controlled reactions were observed [2]. Examples described here include low methanation selectivity in WGS applications and large operating windows for PROX at very high space velocities. A complete reformer system with Microlith ATR, WGS and PROX reactors has been identified. Sensitivity of system size with regard to steam:carbon ratios, and the resulting implications for reactor/heat exchanger sizes were documented and a compact system identified.

Keywords: Microlith; ATR; WGSR; PROX; Fuel processing; Short contact time

1. Introduction

In recent years development of reforming systems for converting hydrocarbon fuels into hydrogen has received increased attention in light of a drive to use hydrogen as fuel for powering fuel cell driven vehicles, auxiliary power units, electronics, etc. With the current lack of a hydrogen distribution network, though, hydrogen will have to be produced locally from traditional fuels, such as natural gas, gasoline, diesel or methanol in relatively small fuel reforming systems.

While steam reforming (SR) and auto thermal reforming (ATR) are well established technologies for converting hydrocarbons into syngas and hydrogen, these reactions are carried out in extremely large, chemical plant size reactors. Scaling them down to the sizes required by fuel cell applications faces significant challenges. Auto thermal reformers balance the heat generated from exothermic reactions with endothermic reactions without transfer surfaces.

Large-scale reformers are often complicated systems. These systems employ oxidation followed by water/steam injection and is often referred to as POX, as opposed to ATR where fuel/air/steam are all injected together. POX and SR systems usually operate at larger scales, and are limited by low power density, sluggish transient response and slow

☆ This paper was presented at the 2004 Fuel Cell Seminar, San Antonio, TX, USA.

* Corresponding author. Tel.: +1 203 287 3700x267; fax: +1 203 287 3710.
E-mail address: sroychoudhury@precision-combustion.com (S. Roychoudhury).
[1] Present address: Columbia University, Earth and Environmental Engineering, S.W. Mudd, Room 926, 500 W 120th Street, New York, NY 10027, USA.

0378-7753/$ – see front matter © 2005 Elsevier B.V. All rights reserved.
doi:10.1016/j.jpowsour.2005.01.051

startup time. Considerable effort has been applied to developing compact and portable fuel reforming systems. While significant progress has been made, a recent paper by Krumpelt et al. [3] highlights the issues that remain to be overcome. Achieving high power density, minimizing the reformer size and cost and improving transient characteristics are some of them.

Catalytic autothermal reforming (CATR) provides an alternative approach to hydrocarbon conversion into hydrogen. In the CATR approach, oxygen is mixed with fuel and steam prior to the reformer. In this case oxidation and reforming reactions occur within the same reactor over the same catalyst, thermally balancing each other. This eliminates the heat transfer limitation of the process and allows the reaction to proceed at much higher space velocities in a much smaller reactor. Unlike traditional ATR reactors, where homogeneous combustion of the fuel rich mixture takes place at the front of the reactor, fuel rich catalytic combustion is employed in the CATR approach. This allows operating in much richer mixtures (lower oxygen to fuel ratio) providing higher efficiency to the reforming process. Also in CATR, steam is added to the fuel/air mixture before entering the reactor eliminating the steam injection step and decreasing the size of the ATR. The SCT CATR process results in reactor power densities much higher than that possible by steam reforming.

The reformate product of the SR or CATR reactor contains between 5 and 15% CO, which cannot be tolerated by proton exchange membrane (PEM) fuel cells and has to be removed from the reformate stream. Generally, water gas shift (WGS) reactors are used to convert CO into additional hydrogen and lowering CO concentration to sub-percent level. Preferential CO oxidation (PROX) reactors are then used to selectively oxidize CO to CO_2 decreasing CO concentration to below 10 ppm, which can be tolerated by a PEM cell. In current technology WGS components comprise about 1/3 of the mass, volume and cost of an integrated fuel reforming system. Therefore, decreasing the size and weight of these reactors is important to meet overall system goals. In PROX reactors high selectivity towards oxidation of CO as opposed to oxidation of H_2 is an important catalyst requirement.

In this work a catalytic autothermal reformer (CATR), a water gas shift (WGS), and a preferential CO oxidation (PROX) reactor based on Microlith catalyst substrate technology was evaluated to determine the advantages offered for the reforming of isooctane and gasoline into hydrogen. The results show the potential for the Microlith technology to significantly reduce the size and weight of these key fuel processor components and associated start-up-time, especially critical for mobile applications.

2. Microlith reactor technology

The Microlith substrate consists of a series of ultra-short-channel-length, low thermal mass, catalytically coated metal meshes with very small channel diameters. The ultra short channel length Microlith substrate minimizes boundary layer buildup and results in remarkably high heat and mass transfer coefficients compared to conventional monolith substrates. The geometry of the substrate provides about three times higher geometric surface area (for supporting catalyst) over conventional reactors (e.g. monoliths) with equivalent volume and open frontal area. The heat and mass transfer coefficients depend on the boundary layer thickness. For a conventional long channel honeycomb monolith a fully developed boundary layer is present over a considerable length of the catalytic surface, limiting the rate of reactant transport to the active sites. This is avoided when short channel length catalytic screens are used. High surface area washcoats have been developed for these short channel substrates by creating a porous ceramic layer from a ceramic powder and a ceramic binder with good interparticle cohesion and adhesion to the substrate surface.

In high temperature reforming reactions the selectivity of the overall process is determined not only by the properties of the catalyst but also by the transport properties of the substrate. The effectiveness of the Microlith technology has been demonstrated in various applications such as exhaust aftertreatment [4], trace contaminant control [5] and catalytic combustion [6]. Microlith-based fuel reforming has been demonstrated via both partial oxidation and auto thermal reforming of gaseous and liquid hydrocarbon fuels (e.g. natural gas [7], propane, diesel, JP-8, Jet-A and methanol [Ref]). Logistic fuels, with high sulfur content, as well as low sulfur diesels and *iso*-octane-based transportation fuels have been examined. Data for an *iso*-octane-based fuel is described here.

3. Catalytic autothermal reforming of *iso*-octane-based fuels—experimental results

Two catalyst formulations were tested for catalytic autothermal reforming of isooctane into hydrogen. One formulation was Pt supported on high surface area La-stabilized *y*-alumina washcoat (Pt–Al) and the other was Rh supported on Ce–Zr washcoat (Rh–CeZr).

For both catalyst formulations the reactors for testing CATR performance were made by stacking individual catalyst coated Microlith screens to a total length between 1.2 and 3.8 cm. A schematic reactor diagram is shown in Fig. 1. The reactor diameter was ∼4 cm (∼1.6 in.). This corresponds to a reactor volume of up to 60 cm^3 and a mass of 46 g. Several thermocouples and gas sampling probes were placed between the screens along the axis of the reactor. This allowed axial temperature and gas composition measurement along the reactor.

The reactor feed was comprised of isooctane (2,2,4-trimethylpentane), steam and air with H_2O/C ratio varied between 0.5 and 2.1 and O/C ratio varied between 0.65 and 1.1. Upstream of the reactor water and air were passed though an electrically heated vaporizer where water was vaporized and

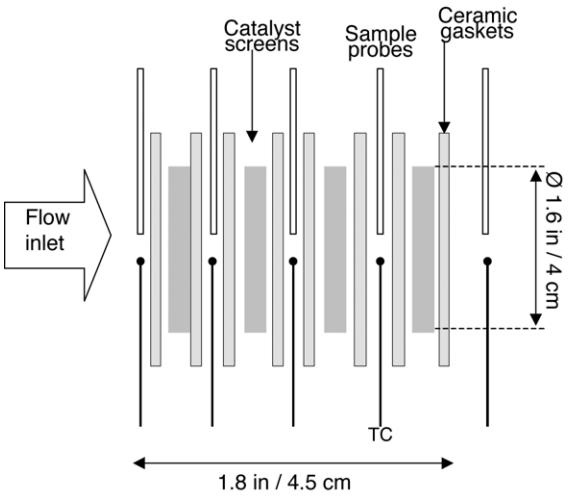

Fig. 1. Schematic diagram of a Microlith-based ATR of isooctane.

mixed with air. Fuel was injected into the stream in a liquid form upstream of a static mixer, where fuel was vaporized and mixed with the stream and air before entering the catalyst bed. The *iso*-octane feed rate, in all tests, was set at 6 ml min^{-1}, and was confirmed by the rate of fuel consumption averaged over the testing time. This fuel flow corresponded to 3.4 kW$_t$ of thermal energy input. Water and air flows were regulated to provide the specified steam to carbon and oxygen to carbon ratios. Water flow was also measured by the rate of water consumption over time and airflow was measured and regulated by a mass flow meter. Gas hourly space velocity (GHSV) of the reactant mixture through the catalyst bed depended both on the number of screens used in a particular reactor and was also varied depending on the test conditions (e.g. space velocity increased at higher O:C and H_2O:C ratios and decreased at lower ratios). In general it varied between about 30,000 and 120,000 h^{-1} for the catalyst beds tested in this study.

Gas chromatography (GC) was used for analysis of the gas samples. Prior to analysis, gas samples were passed through a chiller to remove water and remaining fuel (and/or other non-condensing hydrocarbons formed in the reactor). The gas samples were then analyzed by a GC for H_2, O_2, N_2, CO, CH_4, CO_2 C_2H_4 and C_2H_6 components. Using N_2 as an internal standard and the known molar N_2 input into the reactor (based on the measured inlet air flow) the amount of each component was recalculated into a molar flow rate. The ratio of the sum of CO, CO_2 and CH_4 amounts to the molar input of the fuel into the reactor provided the measure of fuel conversion to C_1 in the reactor, while the ratio of sum of H_2 and CO amounts multiplied by the lower heating value (LHV) of hydrogen to the LHV of input fuel provided the efficiency (assuming 1 to 1 conversion of CO into hydrogen in a downstream WGS reactor).

To start the reactor the catalyst was initially preheated to about 200 °C by flowing hot air through the reactor. Then water and fuel flows were simultaneously started leading to lightoff of the catalyst bed. Thermocouple readings of the

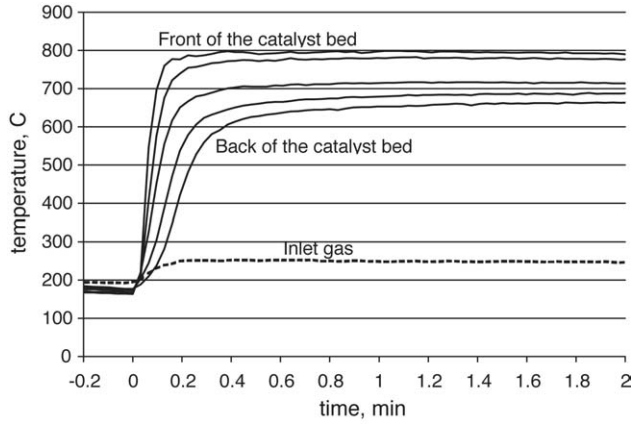

Fig. 2. ATR reactor lightoff (inlet gas temperature vs. catalyst bed temperature) at 120,000 h^{-1}.

catalyst temperature during the start up process are shown in Fig. 2. Fuel and water flows were started at $t = 0$, after which the catalyst bed temperature rapidly increased to a steady state value. From Fig. 2 it can be seen that the start up process took less than 30 s, with the front of the reactor operating after less than 10 s. Note, that the reactor and the test rig were not specifically setup for fast start up measurements. Therefore, initial preheat of the catalyst was limited by the rate of the air heater and by the large thermal mass of the reactor housing.

Initial testing was performed with Pt–Al catalyst using a 1.2 cm (0.5 in.) long catalyst bed at space velocities up to 120,000 1 h^{-1}. The gas composition profiles measured by the probes are shown in Fig. 3. In this test the isooctane flow was set at 6 ml min^{-1} with H_2O:C ratio of 1.5 and O:C ratio of 0.62. These results suggest that the reaction is very fast at the front of the catalyst bed where temperature rapidly rises from an inlet of ∼200 °C to a peak temperature of about 800 °C. All molecular oxygen is rapidly consumed over the first millimeter of the bed length, which causes sharp gradients in all species concentrations.

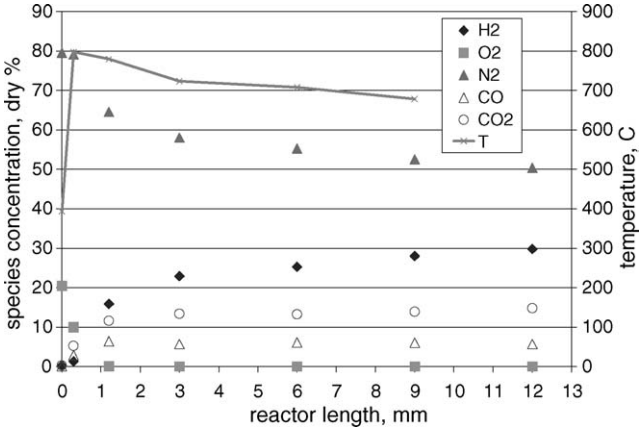

Fig. 3. Concentration profiles along 3.8 cm long Microlith reactor with Pt–Al catalyst at 120,000 h^{-1} at 12 mm, H_2O:C ratio of 1.5, O:C ratio of 0.62 and inlet temperature = 200 °C.

Table 1
Species concentrations for 1.2 cm Pt–Al catalyst bed

O:C	H_2O:C	Peak temperature	H_2	N_2	CH_4	CO	CO_2	C_2H_4	C_2H_6	χ	η
0.62	0.5	831	25.4	52.5	1.38	11.1	9.1	0.23	0.25	47	31
0.62	1.5	797	30.1	50.9	0.72	5.8	14.9	0.03	0.11	49	32
0.8	0.5	864	27.2	48.6	1.03	14.1	7.1	0.18	0.16	68	48
0.8	1.5	845	32.3	46.1	0.72	8.1	13.4	0.03	0.09	71	50
0.98	1.5	883	33.6	43.3	0.52	9.6	12.2	0.01	0.04	94	70
0.98	2	863	34.1	44.1	0.47	7.7	14.0	0.01	0.04	92	66

χ: conversion; η: efficiency.

Similar measurements were conducted over the same catalyst bed at H_2O:C ratio of 0.5, 1.5 and 2.0 and O:C ratio of 0.62, 0.80 and 0.98. The catalyst temperature, species concentration in the exit of the catalyst bed (on a dry basis), fuel conversion and efficiency calculated based on the GC analysis are shown in Table 1. Complete conversion of fuel primarily to H_2 and CO was achieved at a peak catalyst temperature of ~850 °C. In addition, the reactor achieved nearly 90% of the final, or equilibrium, hydrogen concentration within 2 mm into the reactor. Exit mixture composition, for O:C of ~1 and H_2O:C = 2, on a dry basis was 34% H_2, 7.7% CO, 14% CO_2, 0.5% CH_4, 44% N_2 and trace amounts of higher hydrocarbons. There was no evidence of coke formation in the reactor after about 5 h on stream.

A longer bed (~3.8 cm long) coated with the same catalyst was also tested at H_2O:C = 0.5, 1.5 and O:C = 0.82, 0.89 at space velocity of up to 30,000 h^{-1}. The results are presented in Table 2.

Small differences between the results observed between short and long catalyst beds suggest that reforming reactions at the back of the catalyst bed are slow and provide incremental increase in conversion and hydrogen yield at the expense of increased size, weight, catalyst usage and pressure drop. Essentially the front 20 elements provide more than 90% of the conversion, while the rest of the reactor may add less than 10%. This is consistent with the data in Fig. 3, which suggests that very fast reaction occurs on the front of the catalyst bed, especially before molecular oxygen is consumed. Optimization of the process in this region leading to higher selectivity of oxidation reactions to partial oxidation products may increase the overall conversion and efficiency of the process, such that under same inlet conditions 100% fuel conversion is achieved at shorter bed length without increasing the overall size of the reactor.

Test results for Rh–CeZr catalyst obtained on a short catalyst bed screens at space velocities up to 120,000 h^{-1} are shown in Table 3. Comparing these results to the results of Pt–Al catalyst tests suggests that the Rh–CeZr catalyst provides higher conversion and higher efficiency to the process at lower peak temperatures. This is consistent with literature showing Pt favors partial oxidation reactions, while Rh promotes more endothermic steam reforming reactions. Another advantage of the tested Rh-based catalyst over the Pt-based catalyst is in the lower levels of CH_4, C_2H_4 and C_2H_6 yields. In fact, almost no C_2 components were observed under any conditions.

The same reactor was tested for conversion of a blended fuel representing gasoline and consisting of 5 wt.% methylcyclohexane, 20 wt.% of xylene and 75 wt.% of *iso*-octane. The results of this test are shown in Table 4a. It was found that the reactor behavior and the exit gas mixture composition was about the same when running with the blended fuel as with pure *iso*-octane. This suggests that addition of the various hydrocarbons to the fuel did not significantly change the operating properties of the reactor. Comparative performance between *iso*-octane and a blended fuel chosen to represent gasoline for O:C of ~0.6 H_2O:C of ~1.2 shows minor differences in performance and is highlighted in Table 4b.

The results presented in Tables 1–4 suggest that O:C ratio in the inlet mixture is the major parameter determining fuel conversion and process efficiency. To study this dependence a catalyst bed with Rh–CeZr catalyst having length ~3.5 cm was tested under conditions with constant fuel and water feed rate and varying air input. The results of this test are presented in Table 5 and in Figs. 4–6.

Fig. 4 shows the fuel conversion increasing nearly linearly before reaching complete conversion at about O:C = 1. The peak temperature measured within the catalyst increases with O:C ratios as a direct result of increased oxidation reactions. The efficiency, calculated on the basis of LHV of H_2 + CO yielded, peaks at an O/C of 1.07.

Fig. 5 shows the concentrations of hydrogen, carbon monoxide, carbon dioxide, and methane as a function of

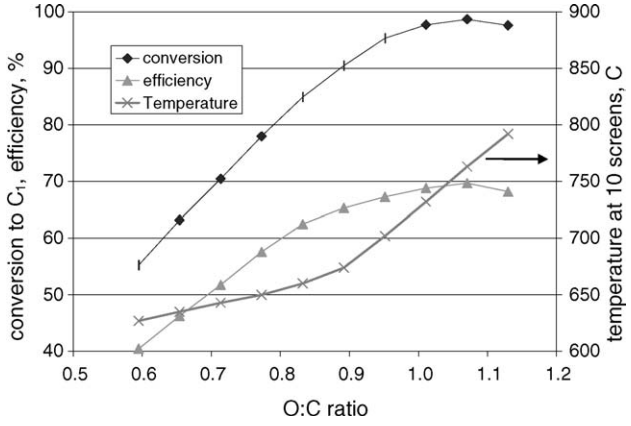

Fig. 4. Conversion, efficiency and peak temperature over the catalyst bed comprised of Microlith elements coated with Rh–CeZr catalyst on washcoat as a function of O:C ratio; H_2O/C of 1.5, space velocity of 55,000 h^{-1}.

Table 2
Species concentrations for 3.8 cm Pt–Al catalyst bed

O:C	H_2O:C	Peak temperature	H_2	N_2	CH_4	CO	CO_2	C_2H_4	C_2H_6	χ	η
0.82	0.51	794	32.5	41.5	1.61	15.4	7.5	0.006	0.045	89	67
0.82	1.22	728	36.8	38.9	1.03	8.2	13.8	0.002	0.020	90	67
0.89	1.24	780	36.0	39.2	0.90	9.9	12.3	0.002	0.011	97	73

χ: conversion; η: efficiency.

Table 3
Species concentrations for 1.2 cm Rh–CeZr catalyst bed

O:C	H_2O:C	Peak temp.	H_2	N_2	CH_4	CO	CO_2	C_2H_4	C_2H_6	χ	η
0.45	0.46	613	36.8	43.3	0.07	9.3	13.1	0.01	0	43	33
0.49	0.46	620	36.9	42.7	0.08	10.9	11.9	0.01	0	49	39
0.52	0.48	626	37.7	44.0	0.09	12.6	10.8	0.0	0.0	52	43
0.55	1.20	621	40.0	40.2	0.08	5.6	16.9	0	0	57	44
0.57	1.20	595	42.7	37.7	0.27	7.3	15.8	0.0	0.0	65	53
0.63	1.20	628	39.7	39.8	0.12	7.3	15.4	0	0	68	53
0.63	1.99	633	39.3	41.5	0.03	3.9	18.0	0	0	62	46
0.71	1.20	621	40.7	37.7	2.04	10.0	13.6	0.0	0.0	91	69
0.88	2.03	700	40.9	40.4	0.44	7.9	15.0	0.0	0.0	95	76

χ: conversion; η: efficiency.

Table 4a
Species concentrations for 1.2 cm Rh–CeZr catalyst bed

O:C	H_2O:C	Peak temperature	H_2	N_2	CH_4	CO	CO_2	C_2H_4	C_2H_6	χ	η
0.60	1.16	640	38.9	39.4	0.078	8.1	15.7	0.00	0.00	68	51
0.60	1.92	637	39.5	39.9	0.048	4.7	18.6	0.00	0.00	66	47

χ: conversion;η: efficiency.

Table 4b
Comparative species concentrations when using *iso*-octane and a blended fuel

Fuel	O:C	H_2O:C	Peak temperature	H_2	N_2	CH_4	CO	CO_2	C_2H_4	C_2H_6	χ	η
Blended	0.60	1.16	640	38.9	39.4	0.078	8.1	15.7	0.00	0.00	68	51
I-octane	0.63	1.20	628	39.7	39.8	0.12	7.3	15.4	0.00	0.00	68	53

Table 5
Species concentrations for 3.5 cm Rh–CeZr catalyst bed

O:C	H_2O:C	Peak temperature	H_2	N_2	CH_4	CO	CO_2	C_2H_4	C_2H_6	χ	η
0.59	1.53	627	36.9	42.1	0.1	3.40	17.5	0.010	0.019	55	41
0.65	1.53	635	37.2	41.3	0.1	3.99	17.4	0.010	0.019	63	46
0.71	1.53	643	37.2	41.1	0.1	4.78	16.9	0.010	0.010	71	52
0.77	1.53	650	37.2	40.7	0.1	5.47	16.4	0.010	0.010	78	58
0.84	1.53	660	36.8	40.8	0.2	6.26	15.9	0	0.010	84	62
0.89	1.53	674	35.9	41.5	0.3	6.85	15.5	0	0.010	90	65
0.95	1.53	702	34.7	42.5	0.4	7.62	14.8	0	0	96	67
1.01	1.53	732	33.6	43.7	0.3	8.19	14.1	0	0	97	69
1.07	1.53	763	32.7	45.0	0.2	8.57	13.5	0	0	98	70
1.13	1.53	792	31.1	47.0	0.1	8.82	12.9	0	0	97	68

χ: conversion; η: efficiency.

the O:C ratio. The methane concentration is seen to pass through a peak at O:C = 0.95, resulting from the relative rates of methane production resulting from decomposition or pyrolysis of the *iso*-octane, and its consumption through reforming and oxidation reactions. It is notable that with increasing O:C, the trends for H_2, CO, and CO_2 concentrations suggest a correlation supported by the reverse water gas shift reaction ($H_2 + CO_2 = H_2O + CO$). This reaction is favored at higher temperatures, which is the effect of increasing O:C seen in Fig. 4.

The reforming of *iso*-octane can be generically represented by the reaction:

$$C_8H_{18} + xO_2 + (16 - 2x)H_2O = 8CO_2 + (25 - 2x)H_2. \quad (1)$$

The reaction stoichiometry shows that the hydrogen yield per mole of *iso*-octane is maximized under steam reforming conditions, when the oxygen-to-fuel (x) or O:C ($2x/8$) is zero. With increasing O:C, the hydrogen yield decreases.

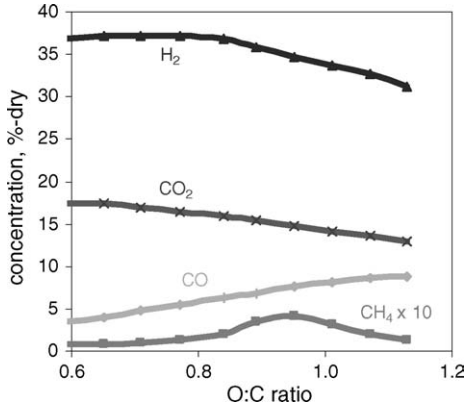

Fig. 5. Concentrations of hydrogen, carbon monoxide, carbon dioxide, and methane from a catalyst bed comprised of Microlith elements coated with Rh catalyst on Ce–Zr washcoat as a function of O:C ratio. H_2O/C of 1.5, space velocity of 55,000 h^{-1}.

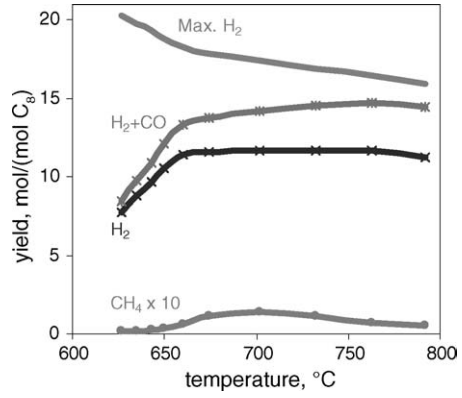

Fig. 6. Yields of hydrogen (H_2 + CO), and methane from a catalyst bed comprised of Microlith screens coated with Rh catalyst on Ce–Zr washcoat as a function of peak temperature. H_2O/C of 1.5, space velocity of 55,000 h^{-1}.

The thermal effect of varying the O:C is quite significant, manifested in the temperatures, which in turn affect the kinetics, conversion, and ultimately the product distribution. Fig. 6 plots the data from Table 5, showing the relationship between the peak temperature and the product yields of hydrogen, H_2 + CO, and methane. The top curve represents the ideal (per Eq. (1)) or maximum hydrogen yield that would be theoretically possible for that experimental condition (measured at the corresponding O:C), and serves as a reference for the experimental output. At low O:C, the temperatures are low, the C8 conversion is low (Fig. 4) and so is the gap between (H_2 + CO) and the maximum H_2 curves. With increasing temperature (O:C), the gap is narrowed because of a convergence of reduced possibilities and increased conversion towards hydrogen and carbon oxides. For these reaction studies (using Rh/CeZr catalyst on a microlith support, with little or no feed preheating), 90% of the theoretical yield of H_2 (assuming each mole of CO can be converted to a mole of H_2) was achievable at an O:C = 1.13, which generated a peak temperature of 792 °C.

Table 6
WGS reactor operating conditions

Test 1: inlet temperature variation: 220, 250, 280, and 310 °C; space velocity = 50000 h^{-1}	
H_2: 41.7%	CO_2: 15.9%
CO: 3.6%	N_2: 29.3%
H_2O: 9.5%	H_2O/CO = 2.64
Tests 2 and 3: inlet temperature variation: 220 and 280 °C; space velocity = 50000 h^{-1}	
H_2: 41.7%	CO_2: 15.9%
CO: 3.6%	N_2: 28%
H_2O: 10.8%	H_2O/CO = 3.0
Tests 4 and 5: inlet temperature variation: 220 and 280 °C; space velocity = 50000 h^{-1}	
H_2: 41.7%	CO_2: 15.9%
CO: 3.6%	N_2: 26.2%
H_2O: 12.6%	H_2O/CO = 3.5
Tests 6 and 7: inlet temperatures of 220 then 280 °C; space velocity variation: 50000, 40000, 30000, 20000, 10000 and 5000 h^{-1}	
H_2: 41.7%	CO_2: 15.9%
CO: 3.6%	N_2: 29.3%
H_2O: 9.5%	H_2O/CO = 2.64

3.1. WGS reactor testing

To ensure a compact fuel processor system can be developed, the water gas shift (WGS) reactor should be designed to operate at its most efficient condition. The concentration of the reactants and products determine the equilibrium point, which limits the kinetics and conversion achievable. In overall system efficiency calculations, the water balance has been recognized as a critical component [8]. Therefore, tests were designed to elucidate the effect of S:C ratio into the ATR, which is manifested in H_2O/CO ratio into the WGS reactor, on the performance of the WGS reactor. Table 6 lists a series of tests that were conducted to study the effect of temperature (exit), H_2O/CO ratio, and space velocity in a Microlith-based WGS reactor. The matrix consisted of seven experimental test conditions; the first five were at a space velocity of 50,000 h^{-1} over a range of temperatures and three different H_2O/CO ratios. Tests 6 and 7 consisted of space velocity variations at 2 different temperatures. For example, test 6 explored the reactor performance at the compositions shown over the space velocity range at an inlet temperature of 220 °C, whereas test 7 did the same at a temperature of 280 °C.

3.2. Water gas shift reactor performance—experimental results

Fig. 7 shows the effect of (exit gas) temperature on CO conversion achieved in the experimental reactor, using a GHSV of 50,000 h^{-1}, an inlet CO concentration of 3.6%, and a H_2O/CO molar ratio of 2.6. The conversion increased from 0.9% at 220 °C to 14% at 310 °C. If allowed to reach equilibrium, the corresponding conversions would be 78% and 32%, respectively.

It is clear that a space velocity of 50,000 h^{-1} is too high for the WGS reactor to reach equilibrium conversions at the

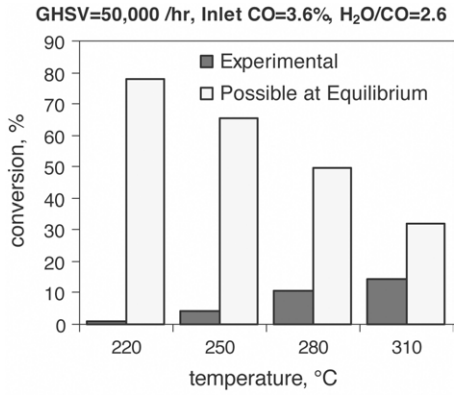

Fig. 7. Effect of temperature on CO conversion achieved in a Microlith-WGS reactor.

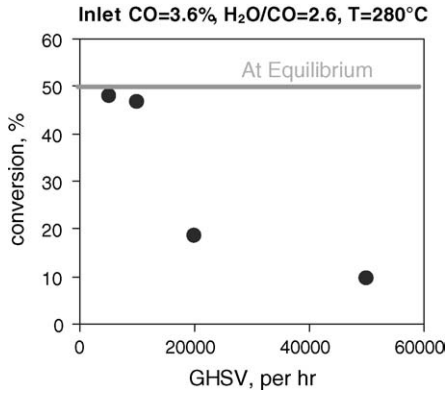

Fig. 9. Effect of the gas hourly space velocity on CO conversion achieved in a Microlith-WGS reactor.

given composition and temperatures. For a given temperature, either lower space velocities need to be employed or the composition needs to be changed such that more water is supplied to the WGS reactor, see Fig. 9.

Fig. 8 shows the effect of the S:C (H_2O/CO) on CO conversion at two operating temperatures. At the lower temperature (220 °C), the conversion jumped from 0.9% to 4.5% when the S:C was increased from 2.6 to 3.0. At the higher temperature of 280 °C, the effect was quite modest in going from S:C = 2.6 to 3.0. Increasing the S:C to 3.5 yielded a significantly higher CO conversion of 28%.

Fig. 9 shows the effect of the gas hourly space velocity on CO conversion. The conversion increased with increasing residence time (lower space velocity), approaching the equilibrium conversion of 49.8%. The effect (slope) appears to be sharpest between the GHSVs of 10,000 and 20,000.

Based on the combination of conditions tested, i.e. inlet temperature, GHSV, and S:C ratio, it would be advantageous to increase the water concentration because that would yield a two-fold benefit. First the equilibrium point of the reaction would move in favor of more hydrogen and second, the kinetic rate would increase by the dependency on the water concentration, which is greater than one to one. For example, it has been shown that a 1% increase in water concentration yields a 10% increase in CO conversion rate, or, conversely, a 10% reduction in WGS reactor size for the same conversion [9].

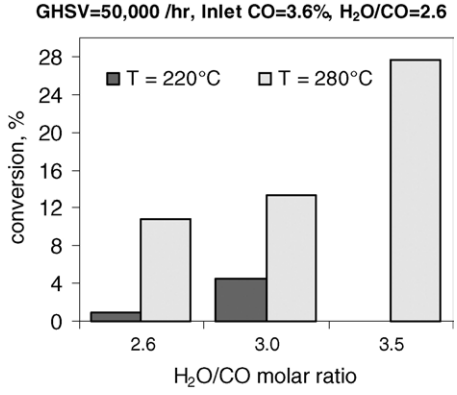

Fig. 8. Effect of S:C on CO conversion achieved in a Microlith-WGS reactor.

To complement and assist in the understanding of the testing, a predictive model was developed under an NSF grant. This model is based on first principles. It uses a kinetic expression specific to the catalyst formulation and transport equations, and calculates changes across each element. Since a SCT reactor is made up of discrete elements, the model takes advantage of that aspect by treating each element separately and determining the changes in conversion, fluid properties and pressure drop across each element. This algorithm allows the model to be extended to any number of elements required by a given reactor to achieve a targeted performance. This is a significant improvement over earlier SCT reactor models. Previous researchers mostly used correlations [10–16]. Another attribute of the model is the calculation of a diffusion coefficient for the reactants in the *actual* gas mixture, not resorting to binary diffusion estimations, which is routinely done. Finally, the model provided the ability to select how closely the reactor operated to the adiabatic or isothermal limits. The outcome of these efforts led to a considerably more accurate model that predicts the transition from kinetic to mass transfer controlled operation and provided a more meaningful prediction of reactor size for a given set of inlet conditions.

Table 7 shows the results of model prediction for various inlet conditions to the ATR. The objective was to provide the WGS with a re formate from the ATR which exited at 700 °C and to determine the conditions that a WGS stage would need to operate to provide an outlet CO concentration of 1%, which could then be fed to a preferential CO oxidation reactor. These conditions were chosen based on analysis of likely heat exchanger performance integrated between the ATR and the WGS. Keeping in mind that the motive was to understand the effect of water on the WGS performance, the O/C ratio was kept constant at 0.9 as the H_2O/C varied from 1.5 to 2.0. Notice that at H_2O/C of 2.0 the O/C had to be adjusted to 1.01 because at that water concentration, a O/C of 0.9 would not achieve an outlet ATR temperature of 700 °C.

Table 7
Results of model predictions for HTS WGS reactor

Inlet to ATR	O/C = 0.9 and H_2O/C = 1.5		O/C = 0.9 and H_2O/C = 1.8		O/C = 1.01 and H_2O/C = 2.0	
	HTS inlet	HTS outlet	HTS inlet	HTS outlet	HTS inlet	HTS outlet
Model predictions for HTS performance						
H_2	31.846	39.810	31.056	37.680	28.130	34.279
CO_2	8.836	16.800	9.280	15.910	9.626	15.776
CO	9.944	1.980	8.494	1.870	7.005	0.855
N_2	31.920	31.920	30.220	30.220	31.396	31.399
H_2O	17.454	9.490	20.944	14.320	23.842	17.691
O/C (overall atom balance)	2.40	2.40	2.70	2.70	3.01	3.01
H/C (overall atom balance)	5.25	5.25	5.85	5.85	6.25	6.25
O_2/N_2 (overall molecular balance)	0.71	0.71	0.79	0.79	0.80	0.80
Temperature (°C) at inlet	310		310		310	
CO Conversion	0.8	0.8	0.78	0.78	0.88	0.88
% conversion of equilibrium	90%	90%	90%	90%	90%	90%
GHSV (reactor assume 80% adiabatic)	20000 h^{-1}	±5000	60000 h^{-1}	±15000	35000 h^{-1}	±10000

The model had been extensively validated for high temperature (HTS) conditions, therefore only the low temperature shift (LTS) conditions required testing. It should be noted, that after testing, the model accurately predicted the experimental results for the LTS conditions. As can be observed from the table, at an O/C ratio of 1.01 and H_2O/C = 2.0, a LTS WGS stage is redundant. The WGS section of the fuel processor therefore can be a *single* stage. This greatly reduces the size and complexity of the system and is a preferred mode of operation.

The experimental data in Table 8 shows the results of testing under the second set (Tests 2 and 3) of WGS reactor conditions. CO conversions were calculated from measured concentrations of CO. Except for N_2, the concentrations of all the other species were calculated from a mass balance using the water-gas shift reaction stoichiometry.

Table 8 also shows the experimental results of the LTS WGS tested under the second set of conditions. The inlet conditions to the LTS reactor do not exactly match the outlet conditions from the HTS reactor because of flow metering limitations. To obtain the theoretical equilibrium CO conversion for the LTS, the actual test inlet conditions were used in the thermodynamic calculation. The reported data for the experimental CO conversion was an averaging of at least four data points taken at each steady state condition and resolving the associated errors. The space velocity targets were 5000, 8000 and 10,000 h^{-1}, however the actual space velocities achieved were a result of flow meter limitations and resolution for the given conditions.

Our results suggest that ATR H_2O/C ratios greater than 1.5 allow efficient WGS reactor design. As can be seen from Table 8 a 20% increase in the amount of water to the WGS will result in a 65% increase in conversion for a given space velocity (0.38 at 6000 h^{-1} at H_2O:C = 1.5 versus 0.62 at 6000 h^{-1} at H_2O:C = 1.8). Conversely this can be viewed as a reduction in reactor size of ∼75% for a given conversion. To determine the optimal steam content entering the ATR, a system level calculation must be done to determine the effect

Table 8
Results of experimental data for LTS WGS reactor

Inlet to ATR	O/C = 0.9 and H_2O/C = 1.5		O/C = 0.9 and H_2O/C = 1.8		O/C = 1.01 and H_2O/C = 2.0
	LTS inlet	LTS outlet	LTS inlet	LTS outlet	
Experimental data					
H_2	40.35	41.11	37.86	39.03	No LTS needed at these conditions
CO_2	16.68	17.44	15.68	16.85	
CO	1.99	1.23	1.88	0.71	
N_2	31.48	31.48	30.26	30.26	
H_2O	9.50	8.74	14.32	13.15	
O/C (overall atom balance)	2.40	2.40	2.71	2.71	
H/C (overall atom balance)	5.34	5.34	5.95	5.94	
O_2/N_2 (overall molecular balance)	0.71	0.71	0.79	0.79	
Temperature (°C) at outlet		260		260	
CO conversion	0.38 ± 0.026	@ 6000 h^{-1}	0.62 ± 0.026	@ 6000 h^{-1}	Outlet conditions are for this GHSV
% Conversion of equilibrium	79%	79%	92%	92%	
			0.60 ± 0.024	@ 8300 h^{-1}	Outlet conditions not shown here for this GHSV
			90%	90%	
			0.56 ± 0.015	@ 10300 h^{-1}	Outlet conditions not shown here for this GHSV
			87%	87%	

of additional steam on fuel processor efficiency. The calculation must include parameters such as pressure drop, reactor size and weight, heat exchanger size and weight and dynamic interaction between the various components comprising the fuel processor. From the WGS evaluation standpoint, it is recommended that a H_2O/C of 2.0 be used since that condition results in a single WGS reactor compatible with use of a PROX reactor for final CO cleanup.

Model calculations indicated that a high temperature shift (HTS) inlet temperature of ∼310 °C was required to produce outlet CO levels of 1.98% and 1.87% respectively for H_2O:C = 1.5 and 1.8 cases. Note that for O:C = 1.01 and H_2O:C = 2.0 case, a 310 °C HTS inlet temperature gave an outlet CO level of 0.855% indicating the potential of operating with only one HTS stage upstream of a PROX reactor. A WGS prediction model, developed and validated at PCI, based upon experimentally established reaction kinetics, was used to predict the space velocities required to achieve 90% of the equilibrium CO conversion for these three HTS cases. The space velocity was predicted assuming that 80% of the heat generated from the WGS reaction was used to raise the temperature in the reactor.

To ensure the integrity of the data obtained for the tests, GC calibrations were done on all species pre- and post-testing. The calibrations were within ±5% of their target concentrations. Mass flow controller calibrations were confirmed post-testing and were within ±2% of calibration. Lastly, the water syringe pump calibration was verified pre- and post-testing and resulted in ±2% error in the targeted calibration. Unfortunately, these and other minor errors prevented a mass balance based on reaction stoichiometry and due to the small changes in large concentrations. For example, the CO_2 GC measurement had an error of 5% associated with it based on the calibration data. Since the CO_2 concentration was in the range of 15%, that led to a range of possible values from 14.25% to 15.75%, or a difference of 1.5% in concentration. The CO concentration, however, started at ∼2% and was consumed to a level of ∼1%, which represents a ∼1% change in concentration. That 1% CO concentration change is within the 1.5% uncertainty in the CO_2 measurement, thus preventing a meaningful mass balance.

4. PROX reactor design—estimations based upon verified performance model

PCIs PROX reactor scaling model was used to calculate the PROX reactor needed to reduce the CO percentage to less than 50 ppm. The scaling model was based upon prior data with these reactors. However, the results were verified for the current case at two conditions. The design flow of reactant into the first stage of the PROX was 266 SLPM, with a wet gas composition of H_2 = 43.9%, CO_2 = 18.1%, CO = 1.4%, N_2 = 29.3%, H_2O = 7.3%. The model identified information such as, the number of stages needed, the quantity of air injected at each stage, the catalyst volume in each stage, inlet/outlet temperatures at each stage, inter-stage gas compositions, extent of methanation, cross-sectional area, pressure drop, etc. The results of the analysis indicated that under very dry conditions (∼7% H_2O entering the PROX) more than three adiabatic stages would be needed to reduce the CO concentration to less than 50 ppm from the inlet conditions provided.

The in-house model developed by PCI for PROX reactor sizing did not use kinetic information to determine the extent of conversion and selectivity. For that reason, it was more of a heuristic model that was verified for reactor scale-up of conditions similar to those tested on the sub-scale level. Our initial assessment was that a two stage adiabatic reactor would not be feasible for the dry conditions because the high hydrogen concentration and the low water concentration. Essentially, to produce an outlet CO concentration of 50 ppm within two stages, the conversion per stage would have to be more than 97%. In addition, to have an efficient design and avoid excessive hydrogen consumption, the reactors would have to be at least 50% selective toward CO oxidation. The inability to achieve these results from a two stage adiabatic reactor under the constraints of such high hydrogen and low water content was experimentally verified. The results are shown in Table 10, which displays the per stage information as well. In addition, there is a “System Totals” box that provides information for all stages as one unit.

Table 9 shows the results of the data generated to achieve less than 50 ppm outlet CO concentration. The first box, labeled PROX 1, shows that about 60% CO conversion for a lambda (defined as $2O_2$/CO) of 1.5 can be achieved with a high selectivity of 88%. Another set of experiments was done where the outlet composition from the PROX 1 experiments were used as input for the PROX 2 experiments. The data is given in the box labeled “PROX 2” and it shows nearly the same CO conversion as PROX 1, yet the selectivity drops considerably to 15%. These conversions achieve only 200 ppm after two stages.

Because of the precipitous drop in selectivity in PROX 2, an experiment for PROX 3 was not done. Instead, two calculations were done. The first was to determine the minimum requirements for a third stage to achieve the desired 50 ppm outlet CO concentration (Table 9, “PROX 3”). This indicated, on the basis of experimental data, that CO conversion of ∼98% would be required in the third stage, which would be unachievable. A second calculation presuming continuous CO conversion of 60%, extrapolating the experimental results from PROX 1 and 2 operated at 110,000 h^{-1} each, predicted six stages would be needed to meet the 50 ppm threshold.

A cursory analysis of inlet conditions to a PROX system indicates that the water content would need to be higher (ATR H_2O:C = 2 and H_2O into PROX at 20%) and lower H_2 entering the PROX (at ∼31%) to result in a two stage compact reactor system. For example, using conditions consistent with WGSR operation that were tested, assuming ATR steam

Table 9
Experimental data and estimates for PROX conditions

Parameters		Comments	Inlet compositions		
			Component	Molar flow rate	Normalized amount
PROX1					
CO in	1.33%	Based on test data at conditions	H_2	0.0863	0.415
CO out	0.56%	Based on test data at conditions	CO	0.0028	0.013
CO conversion	58%	Based on test data at conditions	CO_2	0.0358	0.172
Selectivity	88%	Based on test data at conditions	H_2O	0.0144	0.070
Lambda	1.5	Based on test data at conditions	N_2	0.0664	0.319
Air needed (SLPM)	13.2	Based on test data at conditions	O_2	0.0021	0.010
Tin (°C)	125	Based on test data at conditions			
Tout (°C)	150				
Space velocity (1 h^{-1})	110000				
Area (in.^{2})	28.26				
Volume (in.^{3})	9.3				
Volume (l)	0.2				
Total flow rate (SPLM)	279.20				
PROX 2					
CO in	0.54%		H_2	0.0860	0.403
CO out	0.22%		CO	0.0012	0.005
CO conversion	60%	Optimized value based on test data at conditions	CO_2	0.0374	0.175
Selectivity	15%	Based on test data at conditions	H_2O	0.0147	0.069
Lambda	2.4	Based on test data at conditions	N_2	0.0715	0.335
Air needed (SLPM)	10.4		O_2	0.0025	0.012
Tin (°C)	125	Estimated			
Tout (°C)	130	Estimated			
Space velocity (1 h^{-1})	110000	Estimated			
Area (in.^{2})	12.56				
Volume (in.^{3})	9.6				
Volume (l)	0.2				
Total flow rate (SPLM)	289.56				
PROX 3					
CO in	0.2100%		H_2	0.0821	0.374
CO out	0.0049%		CO	0.0005	0.002
CO conversion	97.7%	Minimum needed	CO_2	0.0381	0.173
Selectivity	5.6%	Minimum needed	H_2O	0.0186	0.085
Lambda	8	Chosen based on PCI database	N_2	0.0784	0.357
Air needed (SLPM)	12.0		O_2	0.0021	0.009
Tin (°C)	125	Chosen based on PCI database			
Tout (°C)	130	Chosen based on PCI database			
Space velocity (1 h^{-1})	285000	Chosen based on PCI database			
Area (in.^{2})	12.56				
Volume (in.^{3})	3.7				
Volume (l)	0.1				
Total flow rate (SPLM)	291.25				

System totals

CO in	1.33%
CO out	49 ppm
Space velocity (1 h^{-1})	46103
Volume (l)	0.4
Volume (in.^{3})	22.7
Total air needed	35.6 SLPM

to carbon ratios of 2, and O:C = 1, it was determined that it would require 2 PROX stages [8].

To conclude, the results of PCIs data analysis and calculations for very dry inlet PROX conditions indicate that more than three stages would be needed to achieve less than 50 ppm outlet CO concentration. In addition, due to the high hydrogen and low water content in the influent, there would be a significant amount of hydrogen consumed during the operation. For a two-stage PROX reactor system, that achieves high CO concentration, and good selectivity, the hydrogen and water content should be selected in context of a system efficiency study that incorporates the trade-offs between additional water input and reactor size, pressure drop and start-up capability.

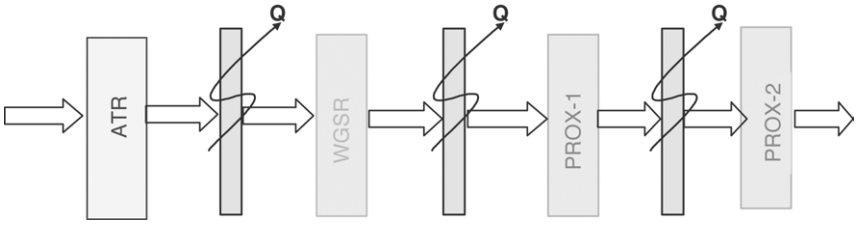

Fig. 10. Schematic of integrated reactors.

The above discussion detailed the performance of the ATR, WGS and PROX reactors individually. The reactors were not tested simultaneously due to constraints of the test stand. Instead, a simulated feed was used to evaluate the performance of the individual reactors. For example, measures from the ATR outlet were simulated using mass flow controllers for the WGS testing. A detailed inspection and analysis of the data and model results indicate that using a O/C = 1.0 and a H_2O/C = 2.0 would allow for a single stage WGS reactor followed by a two stage PROX system, resulting in a CO outlet concentration between 10 and 50 ppmV from the fuel processor. Fig. 10 below shows a conceptual schematic of the overall system design. It is anticipated that the heat removed from streams between reactors would be integrated properly to maintain a high overall system efficiency.

5. Conclusions

An Auto-Thermal Reformer (ATR) based on the Microlith catalyst substrate technology was evaluated to determine the advantages offered for the reforming of isooctane (2,2,4-trimethylpentane) and a blended fuel (5 wt.% methylcyclohexane, 20 wt.% of xylene and 75 wt.% of isooctane) into H_2. Results obtained show the potential of the technology to significantly reduce the size and weight of ATR and associated start-up-time, especially critical for reformer startup. Complete conversion of fuel to C_1 products with efficiencies as high as 80% compared to the thermodynamically predicted maximum value of 91% (assuming downstream conversion of CO into H_2), at an O:C ratio of about 1 and an H_2O:C ratio of about 2 was demonstrated. These results were obtained at space velocities of up to 185,000 h^{-1}. Low methane yield (0.1–0.45%) with almost no C_2 components at maximum bed temperatures of ∼700 °C was observed due to high initial selectivity to partial oxidation products. The data suggests that fuel conversion increases nearly linearly before reaching complete conversion at about O:C = 1.

Based upon these results, the reactor bed weight for a 15 kW_e system is expected to be 132 g (0.3 lbs). The Rh-based catalyst supported on Ce–Zr washcoat was found to provide higher conversion and efficiency than a Pt-based catalyst. The Rh-based catalyst also produced lower methane yield and significantly lower maximum bed temperatures (∼700 °C versus ∼850 °C) due to higher initial selectivity to partial oxidation products (H_2 + CO instead of H_2O + CO_2). Kinetics of the ATR process suggests that for all catalysts the highest reaction rate occurs on the front of the catalyst bed where oxidation reactions take place, followed by slower reformation reactions. Making these fast oxidation reactions more selective towards partial oxidation products may further increase process efficiency.

For the WGS reactor ∼90% of equilibrium CO conversion was observed under Low Temperature Shift conditions at ∼260 °C and space velocity of ∼9000 h^{-1} assuming ATR H_2O/C ratios of 1.5–2.0. In general, a slight increase in water addition to the ATR inlet resulted in a significant decrease in WGS reactor size. Experiments and calculations indicated that, within the range of conditions examined, a small increase in H_2O to the ATR, resulted in a proportionately greater decrease in WGS reactor size. It was determined that H_2O/C ratios greater than 1.5 allow efficient WGS reactor design. At a steam to carbon ratio of 2.0, the Microlith-based WGS reactor was expected to reduce the CO, in a single stage, to below 1%, where a PROX reactor could be used for final CO cleanup.

In order to achieve outlet CO concentration of less than 50 ppm for a given temperature, reformate flow rate (266 SLPM) and low H_2O:C ratio, an in-house model predicted that more than three stages would be needed. As a result of the low water concentration, reactor instabilities were observed which prevented high CO conversion, with good selectivity, to be obtained in two adiabatic stages. In addition, due to the high hydrogen and low water content in the feed to the PROX, a significant amount of hydrogen would be consumed. It was determined that in order to use a two-stage PROX reactor system (space velocities of ∼110,000 h^{-1}) with high CO conversion and good selectivity, the water content of the feed would need to result in a H_2O/C ratio (at the ATR) greater than 1.5 and preferably 2.0.

The results indicate that the incorporation of Microlith-based fuel processor components is likely to result in a compact fuel processor capable of meeting DOEs aggressive start-up-time goals. The results also indicate the necessity of conducting system level studies to address trade offs between overall system efficiency and component size and operability as a function of feed water content.

Acknowledgement

Work supported in part by the U.S. Department of Energy, Office of Energy Efficiency and Renewable Energy, under Contract W-31-109-Eng-38.

References

[1] Microlith Catalytic Reaction System. Patent 5,051,241 (1991).
[2] M.J. Castaldi, US Patent 6,746,657, 2004.
[3] M. Krumpelt, T.R. Krause, J.D. Carter, J.P. Kopasz, S. Ahmed, Catal. Today 77 (2002) 3–16.
[4] S. Roychoudhury, J. Bianchi, G. Muench, W.C. Pfefferle, SAE 971023, SAE International, Warrendale, PA, 1997.
[5] J. Perry, R.N. Carter, S. Roychoudhury, SAE 01-2112, SAE International, Warrendale, PA, 1999.
[6] G. Kraemer, W.C. Pfefferle, J. Ritter, Proceedings of the International Jt. Power Gen. Conference, ASME, 1997.
[7] M. Lyubovsky, H. Karim, P. Menacherry, S. Boorse, R. LaPierre, W.C. Pfefferle, S. Roychoudhury, Catal. Today 83 (2003) 183–197.
[8] S. Ahmed, J. Kopasz, R. Kumar, M. Krumpelt, J. Power Sources 112 (2002) 519–530, Water balance in a polymer electrolyte fuel cell system.
[9] M.J. Castaldi, M. Lyubovsky, R. LaPierre, W.C. Pfefferle, S. Roychoudhury, Performance of Microlith based catalytic reactors for an isooctane reforming system, SAE Technical Paper 2003-01-1366.
[10] J. Armour, J.N. Cannon, AIChE J. 14 (3) (1968) 415–420.
[11] J.P. Reymond, Catal. Today 69 (2001) 343–349.
[12] R.D. Hawthorn, AIChE Symp. Ser. 70 (134) (1974) 428–438.
[13] A.F. Ahlstrom-Silversand, C.U.I. Odenbrand, Chem. Eng. J. 73 (1999) 205–216.
[14] J. Votruba, O. Mikus, K. Nguen, V. Hlavacek, J. Skrvanek, Chem. Eng. Sci. 30 (1975) 201–206.
[15] P. Grootenhuis, ASME (1953) 837–845.
[16] W.-J. Park, D. Ruch, R.A. Wirtz, American Institute for Aerology and Astrology (AIAA) paper no. 2002-0208.